Journal of Neuroscience Methods 205 (2012) 357–363

Contents lists available at SciVerse ScienceDirect

Journal of Neuroscience Methods

journal homepage: www.elsevier.com/locate/jneumeth

Basic Neuroscience

Repeatable target localization for long-term in vivo imaging of mice with 2-photon microscopy

Jasmin K. Hefendehl[a,b,c], David Milford[a], Daniel Eicke[a], Bettina M. Wegenast-Braun[a,b], Michael E. Calhoun[a], Stefan A. Grathwohl[a,b], Mathias Jucker[a,b], Christian Liebig[a,b,*]

[a] Department of Cellular Neurology, Hertie-Institute for Clinical Brain Research, University of Tübingen, D-72076 Tübingen, Germany
[b] DZNE, German Center for Neurodegenerative Diseases, D-72076 Tübingen, Germany
[c] Graduate School for Cellular and Molecular Neuroscience, University of Tübingen, D-72074 Tübingen, Germany

ARTICLE INFO

Article history:
Received 26 August 2011
Received in revised form 27 October 2011
Accepted 31 October 2011

Keywords:
Head fixation device
2-Photon imaging
Alzheimer's disease

ABSTRACT

Repetitive in vivo imaging in mice has become an indispensable tool for studying dynamic changes in structure and function of the brain. We describe a head fixation system, which allows rapid re-localization of previously imaged regions of interest (ROIs) within the brain. Such ROIs can be automatically relocated and imaged over weeks to months with negligible rotational change and only minor translational errors. Previously stored imaging positions can be fully automated re-localized within a few seconds. This automated rapid and accurate relocation simplifies image acquisition and post-processing in longitudinal imaging experiments. Moreover, as the laser is only used for data acquisition and not for finding previously imaged ROIs, the risk of laser induced tissue damage and photobleaching is greatly reduced. Thus, here described head fixation device appears well suited for in vivo repetitive long-term imaging in rodent brain.

1. Introduction

In vivo 2-photon imaging of the brain has led to an increased understanding of many fundamental processes such as dendritic spine turnover (Grutzendler et al., 2002; Yang et al., 2009), glial motility/activation (Nimmerjahn, 2005; Davalos et al., 2008), and neural activity (Trachtenberg et al., 2002; Dombeck et al., 2007; Busche et al., 2008) as well as early events in neurodegenerative disease progression. For example, in studies of mouse models of Alzheimer's disease-related pathology, in vivo 2-photon imaging has produced substantial novel findings including β-amyloid plaque dynamics, and plaque-associated local toxicity, e.g. dendritic and spine abnormalities or alterations in calcium homeostasis (Bacskai et al., 2001; Meyer-Luehmann et al., 2008; Busche et al., 2008; Dong et al., 2010). An essential and unifying prerequisite for longitudinal studies of dynamic processes in vivo is the ability to image the same brain volume repetitively over long periods with great precision. Thus, for repeated imaging of the same positions, it is desirable to reliably identify an origin for the coordinate system that contains the positioning information in all three dimensions.

In most existing protocols, the head fixation allows for rotation in some or all planes (Nimmerjahn, 2005; Nase et al., 2005; Bolmont et al., 2008; Meyer-Luehmann et al., 2008; Holtmaat et al., 2009; Judkewitz et al., 2009; Yang et al., 2010; Sigler and Murphy, 2010; Kelly and Majewska, 2010; Spires-Jones et al., 2011). These rotations and additional translational changes have to be compensated for in order to be able to align and compare brain volumes between imaging sessions.

One solution, to overcome positioning errors, is to mark relatively stable biological entities, such as blood vessels or labeled neurons and use them as landmarks. These landmarks can either be used to relocate to a position under visual control or to correct possible rotational or translational shifts between imaging sessions in the post-imaging analysis process (Meyer-Luehmann et al., 2008; Bolmont et al., 2008; Holtmaat et al., 2009; Kelly and Majewska, 2010; Spires-Jones et al., 2011). However, relocation with the aid of landmarks by a visual narrow down approach and comparison of previous images is time-consuming and thereby increases the time the animal needs to be under anesthesia. It also often involves the usage of the laser which might cause photobleaching and tissue damage by heat absorption or phototoxicity. Furthermore, in all approaches involving landmarks the labeling occupies an additional fluorescent channel that could otherwise be used for additional analysis.

Another option to reliably acquire the same data set, without loss in each imaging session, could be to image larger areas to

* Corresponding author at: Department of Cellular Neurology, Hertie-Institute for Clinical Brain Research, University of Tübingen, D-72076 Tübingen, Germany. Tel.: +49 7071 29 87606.
E-mail address: christian.liebig@medizin.uni-tuebingen.de (C. Liebig).

0165-0270/$ – see front matter © 2011 Elsevier B.V. All rights reserved.
doi:10.1016/j.jneumeth.2011.10.029

ensure that all relevant data is still captured within the 3D volume. This enables one to compensate for possible changes in the post-processing analysis without losing data. However, enlargement of the imaged area while keeping the same resolution extends imaging time and laser usage on the tissue, increasing the overall risk of tissue damage by heat or phototoxicity.

Taking the above issues into consideration we present a novel head fixation system that allows fixing a co-ordinate system on the first day of imaging. Stored ROIs can then be quickly and automatically re-located with negligible rotational and only minor translational changes in subsequent imaging sessions.

2. Methods

2.1. Head fixation device

The head fixation stage is mounted in the 2-photon microscope setup and consists of a horizontal fixation plate mounted on two aluminum blocks and a resting plate for the animal (Fig. 1A). A titanium ring (14 mm outer diameter; 0.73 g) is permanently fixed to the mouse head over a cranial window (4 mm in diameter). The titanium ring has a counterpart mounted under the 2-photon microscope (Fig. 1B) immobilizing the mouse during the imaging procedure. In order to control for rotations in all planes, yaw, pitch and roll (Fig. 1C), the titanium ring has a frontal guide notch and a circular guide groove (Fig. 1D), which slides into the horizontal fixation plate within the imaging setup (Fig. 1E and F). The guide groove and notch ensure that the animal's head is always fixed at the same angles during imaging sessions. The anesthetized mouse can be easily restrained and fixated by sliding the titanium ring into the horizontal fixation plate and closing the attached swivel fixation plate with a clamping bolt (Supplementary Movie 1) to secure the titanium ring. The use of only one clamping bolt also minimizes shifts that might be caused by tightening several screws (Dombeck et al., 2007; Hadlock et al., 2007). The rigid head fixation setup will not change during the imaging process. The mouse rests on a heating pad to control body temperature during anesthesia. The mouse is anesthetized with 1–1.5% of isoflourane, which is delivered by a custom made anesthesia mask.

2.2. Automatic re-localization

The horizontal fixation plate is mounted on a motorized *x*–*y* stage, with parts from the integrated in vivo bridge (380FM-2P; Luigs & Neumann, Ratingen, Germany) removed to accommodate the new system. In order to ensure that any saved co-ordinates are re-usable for subsequent imaging sessions, the stage must have a reliable reference position. In our case the stage is set to zero by moving it to the top-right corner (*xy* limit) prior to each imaging session. Alternatively, one could initialize the stage using an electromechanical reference system (e.g. by using linear encoding) or a software based calibration using an optical reference on the stage (Jin et al., 2011). Once the stage is initialized and the animal is head fixed, previously stored positions can be quickly re-located without usage of the laser. The repositioning from one completed position to the next position can be done without any further corrections.

2.3. Material for head fixation stage and assembly

2 aluminum block of 100 mm × 40 mm × 25 mm (A)
2 aluminum block of 100 mm × 80 mm × 27 mm (B)
2 aluminum cylinders of 182 mm in length and 60 mm diameter (uprights)
1 aluminum block of 160 mm × 160 mm × 55 mm (support platform)
1 aluminum plate of 228 mm × 40 mm × 2 mm (stable plate)
1 aluminum plates of 65 mm × 15 mm × 2 mm (swivel plate)
4 aluminum plates of 40 mm × 15 mm × 2 mm
1 aluminum disc 5 mm diameter and 5 mm thick
1 (or as desired) titanium disc 14 mm diameter and 2 mm thick (fixation ring)
4 grub screws 4 mm diameter and 10 mm long (C)
2 steel screws 6 mm diameter and 25 mm long (D)
2 steel screws 6 mm diameter and 30 mm long (E)
1 copper cylinder of 10 mm diameter and 40 mm long (clamping bolt)

The sizes may vary depending on the motorized stage and microscope used. For example in our setup, the height of the upright aluminum cylinders was chosen to make use of the full working distance of the objective in relation to the cranial window without touching it. Following the designs described in the technical drawings (Supplementary Fig. 1) attach A to the motorized stage using screws D. Connect the uprights to B using screws D. Slid B into A and fix with the grub screws (C). Do not over tighten the screws, as it will deform the aluminum of B, which will in turn stop the ease of removal and replacement of this system. Place the support platform on both uprights ensuring the trough lies below the top of the uprights. Over this, place the fixation plate (with connected swivel plate, brace plates and aluminum disc attached) and connect it to the support platform and uprights using screws E (see Supplementary Fig. 1 for detailed technical drawings).

2.4. Cranial window and fixation of the titanium ring

In the present study APPPS1 transgenic animals were used to evaluate the system under in vivo conditions. β-Amyloid deposits were visualized in vivo by intraperitoneal injection of the amyloid-binding dye Methoxy-X04 24 h prior to each imaging session. All experimental and surgical procedures were performed in accordance with the policies on the use of animals in neuroscience research of the Society for Neuroscience and German Law. The mice were weighed to determine the appropriate amount of anesthesia administered by intraperitoneal injection (Fentanyl 0.05 mg/kg, Midazolam 5 mg/kg, Medetomidin 0.50 mg/kg). The animals were placed on a warming pad to maintain a body temperature of ∼37 °C during surgery. The hair was shaved off the complete scalp down to the neck with a small rodent razor. The mice were fixed in a stereotactic frame and both eyes were lubricated with a drop of eye ointment to prevent them from drying. A midline scalp incision was performed extending from the neck region to the front of the head between the eyes. The region of the craniotomy was outlined with forceps using a custom made cover slip as a template. We then drilled along the outline taking care not to use too much pressure and to pause regularly in order to prevent heat generation. A thin layer of bone was left after the drilling process. To test if the bone was thin enough the middle of the craniotomy was touched with forceps. If the bone could be pushed down easily the drilling process was completed. A drop of PBS was put onto the craniotomy to gently remove the left over bone with forceps in order to expose the skull. Great care was taken not to injure the dura mater. A cover slip was put onto the dura mater and gently pushed down until it was flush with the skull. Dental cement (iBond, Heraeus) was used to secure the cover slip to the skull surface. The titanium ring was mounted above the craniotomy using superglue (Sekundenkleber, Uhu). The inner part of the titanium ring was glued to the existing layer of dental cement. Dental cement was also used to support the titanium ring from the outside to further increase stability of the system. Two to three interrupted sutures were performed at the front of the head and the neck until the skin surrounding the titanium ring was completely closed

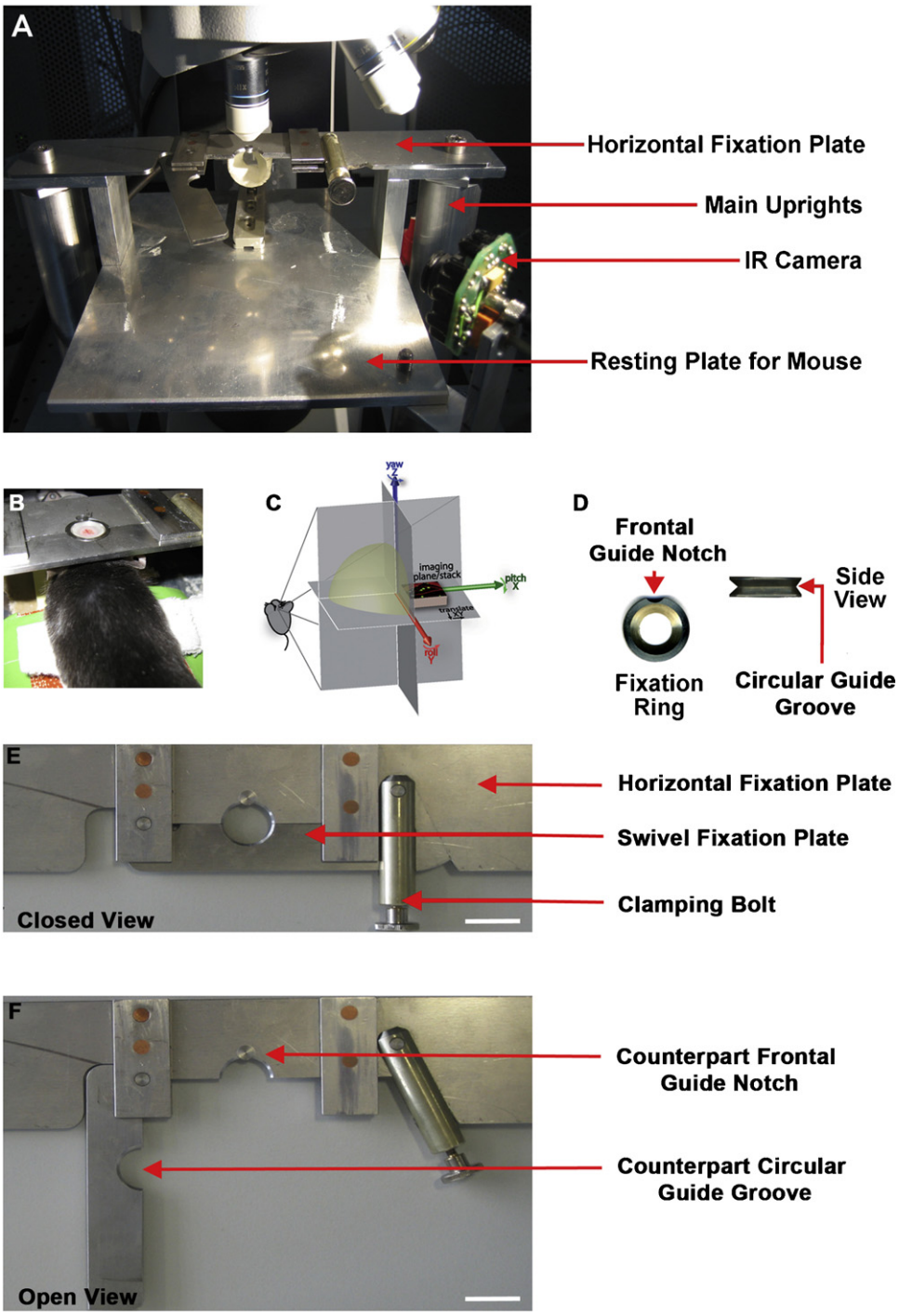

Fig. 1. (A) Fully constructed fixation device under the 2-photon microscope with an infrared camera used to monitor the animal during the imaging progress. (B) Mouse with titanium ring fixed to the horizontal fixation plate under the 2-photon microscope. (C) The guide notch and groove of the titanium ring and the respective counterparts of the horizontal fixation plate reduce tilting in all 3 dimensions (yaw, pitch and roll). (D) Titanium ring for fixation to mount onto the mouse (top and side views). (E) Main horizontal plate for fixation (closed (E) and open (F) view; scale bar = 15 mm). The construction can be done with standard metal shop equipment (lathe/milling/saw), and reasonable time/material expenditures.

(see Supplementary Fig. 2). Appropriate amounts (equal to amount of anesthesia) of antidote were administered (Flumazenil 0.5 mg/kg (Fresenius Kabi), Atipamezol 2.5 mg/kg (Atipam, Albrecht) half by subcutaneous injection and half by intraperitoneal injection. Analgesia in combination with sterile saline was administered (e.g. Temgesic 0.1 mg/kg) by intraperitoneal injection. The mice were monitored until they were fully awake and mobile again and were then returned to their housing cage. We recommend a recovery period of 4–5 days before imaging to ensure that the surgery was successful. If the surgery was not performed correctly it can lead to bleedings or thickening of the dura mater. Both will have a negative impact on imaging quality.

Using this surgery protocol we could not detect inflammation in histological sections stained for Iba-1 directly after surgery in comparison to a control animal, which has not received surgery (Hefendehl et al., 2011). Furthermore, microglia cells were imaged

for up to 6 months in a recent study to ensure that the surgery does not induce long-term changes in morphology (Hefendehl et al., 2011).

2.5. Other surgery techniques

We also used the titanium ring in combination with other surgical methods, e.g. thinned skull preparations. As the shape of the titanium ring provides a stable cavity, open skull preparations can also be performed for electrophysiological experiments, using the titanium ring as a frame for the silicon seal (e.g. KWIK-Cast Sealant, Word Precision Instruments). A comparable design has been published by Judkewitz et al. (2009) lacking however the features to eliminate potential rotation. For cranial window preparations and thinned skull the titanium ring provides a stable bath for objective immersion. For our purposes (see e.g. Hefendehl et al., 2011) we predominantly perform a bi-hemispherical cranial window and mount the titanium ring in the middle of the skull. However, our head fixation system is also used on one hemisphere only to image barrel cortex. This experiment is performed in awake mice showing that the head fixation device is stable enough to support studies in awake animals. (Personal communication with C. Schwarz and B. Joachimsthaler, Systems Neurophysiology, Hertie Institute for Clinical Brain Research, Tuebingen.)

2.6. Animal welfare

Animal caretakers and scientists monitor the animals on a daily basis. No obvious change in behavior or restriction in movement was observed (Supplementary Movie 2). Animals, which received surgery at about 3 months of age, have reached the lifespan of littermates that did not receive surgery. A device that is permanently attached to a mouse's head should account for 5% of total body weight or less (Local Animal Care and Use Committee). Assuming a mouse weight of 25–30 g the titanium ring accounts for 2.4–2.9% of the total body weight. After approval by the local Animal Care and Use Committees and in accordance with the veterinary office regulations of Baden–Wuerttemberg (Germany) the first surgery was monitored by a veterinarian who approved the procedure.

2.7. Microscope

We use a Leica DMLFS microscope equipped with a TCS SP2 scan head (Leica Microsystems, Bensheim, Germany) and a Spectra Physics (San Jose, California) Mai-Tai BB laser, which provides multiphoton excitation from 710 nm to 990 nm (e.g., 810 nm for Methoxy-X04 and 910 nm for Texas Red). Detection was done with two non-descanned PMT detectors within close proximity of the objective. Excitation and emission were separated by a beamsplitter at 725 nm, reflected excitation light was blocked by a short-pass filter at 750 nm. The signal was splitted between the two PMTs at 560 nm.

3. Results

To estimate the accuracy of the head fixation we performed 2 sets of ex vivo measurements using InSpeck Green fluorescent beads (2.5 μm, Invitrogen, Darmstadt, Germany) on an object slide. A titanium ring was glued to the object slide and put into the head fixation device. First we determined the precision of the microscope system itself, then we measured the precision when using the head fixation device, i.e. the sample was removed from and replaced into the device between scans (Fig. 2A). Additionally, we imaged plaques in vivo in APPPS1 mice attached to the head fixation system in order to estimate how the measured precision of the head fixation system relates to geometrical changes based on biological causes (Fig. 2B and C).

All scans were performed as 2-photon scans using a 40× water immersion objective (HCX APO L40×/0.80 W U-V-I, Leica, Bensheim, Germany) with a voxel size (x, y, z) of 0.1 μm × 0.1 μm × 0.5 μm for ex vivo experiments and 0.1 μm × 0.1 μm × 1 μm for in vivo experiments.

All measurements were performed by tracking the movement of the investigated objects (beads or plaques) during a series of scans using Imaris 7.1.1 (Bitplane, Zurich, Switzerland). The estimated positions were exported as x, y and z coordinates into Microsoft Excel for further calculations. One value was calculated for each degree of freedom (3 translational and 3 rotational) for each scan based on the mean of all object positions and vectors available. Thus, the n number given for each set of experiments represents the number of scans. The translational precision is presented as the xy displacement and the z displacement of single objects. The rotational precision was measured by creating vectors connecting the objects and estimating the change of the angle for each vector during a series of scans. All measurements are presented as mean (±SEM).

3.1. Precision of microscope and stage

In this set of measurements we performed four experiments with the sample not being removed during a series of scans to avoid imprecision induced by removing and replacing the sample. Thus the measurements can be used to estimate the intrinsic precision of the microscope system. Several series' of scans were made after switching on the system to estimate the warm-up time needed to avoid thermal drift. All following measurements were done after allowing the system to warm up for this time (3 h, data not shown). After this time there was still a translational displacement of 0.35 (±0.02) μm in xy and 0.06 (±0.01) μm z per 20 min measurable (Fig. 2D, $n = 13$). However, this was constant over several hours so we regard this as the baseline precision of the microscope system. We then investigated whether reinitialization of the microscope causes additional imprecision as it involves movement of the z-drive and the scanning optics. As expected, with a displacement of 0.53 (±0.09) μm in xy and 0.15 (±0.05) μm in z the precision of the stage after reinitialization is somewhat lower than without (Fig. 2E, $n = 6$). Furthermore, movement of the stage might cause an additional error in xy. Thus, we repeatedly imaged a set of stored positions on the same sample without reinitialization and measured a translational displacement of 0.36 (±0.08) μm in xy and 0.07 (±0.01) μm in z (Fig. 2F, $n = 6$).

In our images, a rotation of about 0.05 degree would result in a shift of less than 1 pixel on one side of the image if the center of rotation was on the opposite side. All values obtained for rotation in this set of measurements were at least a magnitude below this value and thus below the detection limit.

3.2. Precision of the head fixation device

To address the precision of the head fixation device itself, we mimicked the normal usage while using an ex vivo sample. We imaged single positions without moving the stage while only removing and replacing the sample with the titanium ring between scans. The measured translational displacement was 4.76 (±0.88) μm in xy and 0.50 (±0.08) μm in z (Fig. 2G, $n = 10$). The angle of displacement around all 3 axes was below 0.02 degree (yaw: 0.016 (±0.008) degree, pitch: 0.005 (±0.001) degree, roll: 0.004 (±0.001) degree) and can be regarded as negligible (Fig. 2H, $n = 10$).

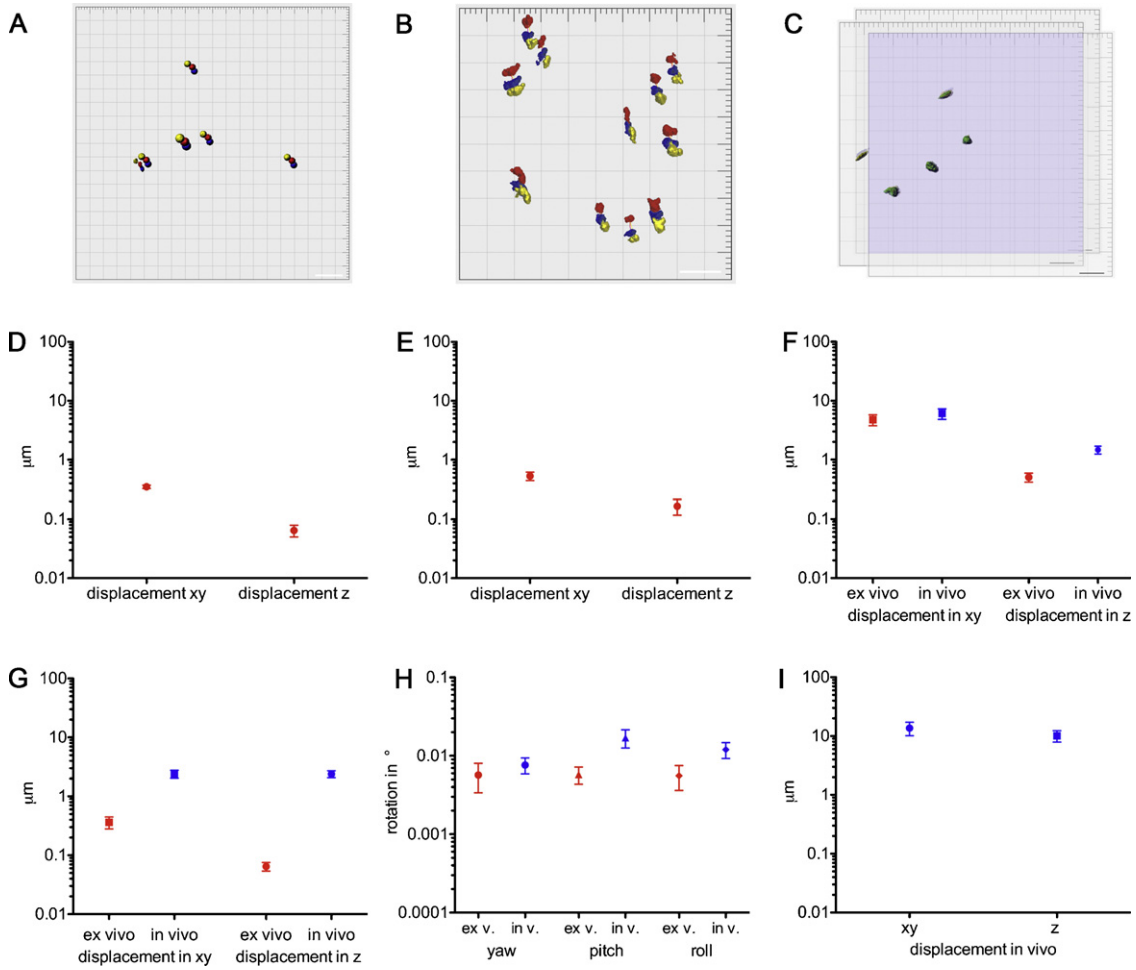

Fig. 2. (A) Surface renderings of detected fluorescent beads, ex vivo, of three scans (represented by 3 different colors) illustrating the shift caused by the removal and subsequent replacement of the ring. The error shown consists of the error of microscope and head fixation not including biological shifts. Scale bar 15 μm. (B) Surface renderings of detected amyloid plaques in vivo in three subsequent scans (represented by 3 different colors) illustrating the shift caused by the removal and subsequent replacement of the ring. The error shown consists of the error of the microscope and head fixation together with biologically caused shifts. Scale bar 15 μm. (C) Surface renderings of detected amyloid plaques in vivo on three subsequent days. This demonstrates the combined shift generated by biological factors as well as the error of the system. The blue area indicates the region that can be used for target localization or analysis without manual adjustments. Scale bar 15 μm. (D) Intrinsic error of the microscope. Leaving ex vivo samples under the 2-photon microscope for 20 min causes a displacement in *xy* and *z*. All other measurements shown include this intrinsic error of the microscope ($n = 13$). (E) Reinitialization of the microscope without any stage movement causes a displacement in *xy* and *z* ($n = 6$). (F) Measurement of the error caused by the movement of the stage. Displacement is determined in *xy* and *z* with an ex vivo sample (red, $n = 6$) and in vivo (blue, $n = 12$). The difference in the detected shift between the ex vivo and in vivo situation of approximately 2 μm originates in the movement of the brain in the in vivo situation. The ex vivo sample demonstrates the error of the system itself. (G) Error caused by removal and replacement of the sample. The in vivo shift is larger by 2 μm in comparison to the ex vivo sample caused by the movement of the brain ($n = 10$ (ex vivo), $n = 12$ (in vivo)). The ex vivo sample demonstrates the error of the system itself. (H) Ex vivo (red, $n = 10$) and in vivo (blue, $n = 12$) measurements of rotational changes along all axes. *xy* around *z* = yaw, *yz* around *x* = pitch, *xz* around *y* = roll. Data was determined by removal and subsequent replacement of the ring with ex vivo and in vivo samples. (I) Measurement of the error caused by removal and replacement of the mouse in a long-term experiment over 3 weeks ($n = 15$).

3.3. *Influence of biological factors*

Knowledge of how the imprecision induced by using the head fixation device, described here within, relates to imprecision induced by biological factors is of great interest. Biological factors can be due to passive movement, e.g. by handling the animal, but also due to developmental processes like growth or swelling. The former would have an influence on the short timescale, the latter over longer periods of time. We performed experiments addressing both forms. All displacement measurements were done on 2 APPPS1 mice, one male (6 months old) and one female (17 months old).

To measure the impact of short time changes that might be induced by moving the animal, we performed an experiment where the animal was left in the head fixation device while scanning a set of predefined positions several times. Here we saw a translational displacement of 2.40 (±0.37) μm in *xy* and 2.39 (±0.32) μm in *z* (Fig. 2F, $n = 12$). For the angle of rotation measured between subsequent scans of a series we obtained 0.008 (±0.001) degree for yaw, 0.023 (±0.008) degree for pitch and 0.012 (±0.002) degree for roll. In a second experiment we imaged the same position subsequently several times, taking the animal out and putting it back into the head fixation device between the scans. We obtained a translational error of 6.06 (±1.22) μm in *xy* and 1.47 (±0.22) μm in *z* (Fig. 2G, $n = 12$) and a rotational error of 0.013 (±0.004) degree for yaw, 0.023 (±0.006) for pitch and 0.021 (±0.004) degree for roll (Fig. 2H).

Because the described head fixation device is designed for long-term longitudinal studies, a test on the impact of long-term biological changes was performed. To this end, we tracked the positional change after storing the position over a period of 20 days. Imaging of the stored positions was done on day 1, 2, 6, 13 and 20. The average translational change between sessions was 13.65 (±3.54) μm for *xy* and 10.11 (±2.19) μm for *z* (Fig. 2I, $n = 15$), with

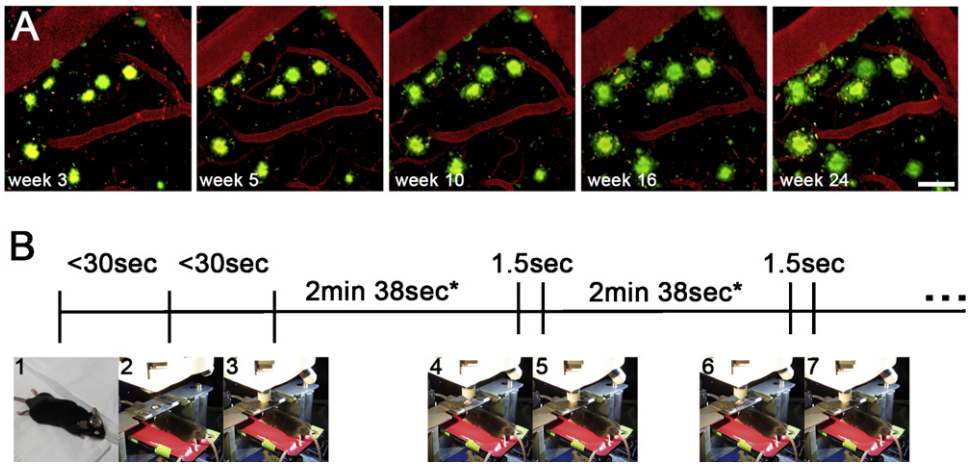

Fig. 3. (A) Long-term imaging of APPPS1 transgenic mice for up to 25 weeks (Hefendehl et al., 2011). Same region of interest is shown with amyloid deposits (green) stained with methoxy-X04, and blood vessels (red) made visible by Texas Red® dextran. A maximum *z*-projection is shown for the imaged volume including truncated plaques located at the rim of the volume. Scale bar 50 μm. (B) Timeline of imaging session including head fixation and re-localization of ROIs. (1) An anesthetized animal can be fixed under the 2-photon microscope in under 30 s ($n = 10$). (2) Adjusting the right objective and re-localization of a previously stored position can be done in under 30 s. (3) Imaging a *z*-stack of 100 μm (*100 Hz, bi-directional, Format 1024 × 1024, *z*-step 1 μm) is performed in 2 min and 38 s. (4) Automatic re-location to the next previously stored ROI takes 1.5 s on average ($n = 12$).

the numbers for the larger time intervals higher than for the short intervals (data not shown). For the rotational change we obtained 0.046 (±0.016) degree for yaw, 0.208 (±0.095) degree for pitch and 0.114 (±0.036) degree for roll ($n = 10$). In an addition we reused data obtained during a previously published study (Hefendehl et al., 2011). The study included eight mice (4 males and 4 females, 3–4 months of age at the beginning of the study) in which we were able to use automatic relocation to identify target regions without the need of enlarging the field of view for up to 25 weeks. In this set of experiments we used Texas Red labeling of the vasculature alongside plaque labeling (Methoxy_XO4) as an additional landmark to verify the locations (Fig. 3A). During this series biological shift did not cause any rotational change that had to be corrected in post-processing. Small manual corrections were sufficient to compensate for translational changes that occurred during the months of the experiment and could always be completed in less than 30 s. Due to the quick and easy re-positioning, we were able to image six brain regions per mouse per imaging session, each having a volume of 0.0171 mm^3.

3.4. Time needed for relocating

While performing in vivo experiments we also measured the time needed for placing the animal in the head fixation device and automatic relocating to previously stored positions (Fig. 3B). Picking the animal up after cleaning the cranial window and placing it in the head fixation always took less than 30 s ($n = 10$; Supplementary Movie 1). The same time accounts for relocating to the first stored position and starting the scan (Supplementary Movie 3). Switching between stored positions took 1.50 (±0.15) s ($n = 12$).

It is important to note that our results are based on the precision and intrinsic error of the microscope and the motorized *x*–*y* stage used as shown in Fig. 2D. If other systems are used the results might vary in respect to a different intrinsic error of the setup. Hence, it is advisable to estimate the intrinsic error of the system before installing the described setup. For troubleshooting during the use of the setup (see Supplementary Table 1).

4. Discussion

The objective of the designed head fixation device was to optimize automated re-positioning in longitudinal imaging experiments by minimizing rotational and translational changes and speeding up the process of relocation. Rotations in all planes could be minimized to a negligible degree. Thus, when automatically repositioning to previously stored locations, without the use of the laser or any other visual guidance, the target location could always be identified reliably. This elimination of geometric changes between imaging sessions simplifies the post-imaging analysis, e.g. alignment of ROIs from different time points. Even though numerous head fixation systems have been reported in the past (Nase et al., 2005; Nimmerjahn, 2005; Meyer-Luehmann et al., 2008; Bolmont et al., 2008; Holtmaat et al., 2009; Judkewitz et al., 2009; Yang et al., 2010; Spires-Jones et al., 2011) the control for geometrical changes during and among imaging sessions has not been shown to the extent presented here. An important factor for the successful control of rotations in the head fixation device presented is the use of a titanium ring with a frontal guide notch and circular guide groove permanently attached to the mouse head with dental cement. The custom build counter parts within the horizontal fixation plate secure the titanium ring in the microscope setup and ensure that the animal is head fixated at identical angles between imaging sessions.

While rotational changes induced by the head fixation device are negligible, some translational changes between imaging sessions still remain. These changes (ex vivo data) are distinctly smaller than the biological changes (in vivo data). By reducing the geometrical changes between imaging sessions mainly to biological variance the precision of the head fixation system allows for easy and reliable relocation. Hence, it saves the experimenter the time needed for tracking, re-localization or comparison of previously imaged ROIs. Furthermore, the reduction of laser (or ambient illumination) usage due to the automatic re-localization is of benefit for the experimental animal as the overall time spent under anesthesia is shortened as well as the exposure of brain tissue to laser (or other) excitation. The use of dental cement and light titanium material enables the permanent fixation of the ring to the mouse head without the use of screws, which could potentially harm the brain and add on weight to the system. The fast automatic re-positioning in combination with a cranial window of 4 mm in diameter allows choosing several ROIs from a relatively large area of the cortex.

We also demonstrated the applicability of the head fixation device for long-term use over up to 25 weeks. There was no need to correct for any rotational change during these weeks and

translational shifts could be corrected in less than 30 s. Thus, we present a reliable and highly efficient imaging setup for longitudinal in vivo studies by 2-photon microscopy.

Author's contribution

D.M. and D.E. have designed and constructed the head fixation system. J.K.H. and S.A.G. have established the cranial window surgery. Imaging was performed by C.L., J.K.H and B.M.W.-B. Evaluation of the head fixation system was performed by J.K.H. and C.L. Experimental design and manuscript preparation were carried out by C.L., J.K.H, M.J., D.K.M, B.M.W.-B., and M.E.C.

Acknowledgements

The authors would like to thank Hubert Willmann and Klaus Vollmer (Precision Mechanics Group, Ophthalmologic Clinic, University of Tübingen) for the construction of the head-fixation system; Rüdiger Berndt for construction of the infrared camera; Tristan Bolmont and Florent Haiss for early discussions of surgical preparation and head-fixation design; Cornelius Schwarz and Bettina Joachimsthaler for their information concerning additional applications of the head fixation system.

This work was supported by European Union FP7 HEALTH (Project LUPAS, M.J.), PhD grant from the charitable Hertie Foundation (J.K.H.) and a Alzheimer's Association Grant IIRG-05-13464 (M.E.C.).

Appendix A. Supplementary data

Supplementary data associated with this article can be found, in the online version, at doi:10.1016/j.jneumeth.2011.10.029.

References

Bacskai BJ, Kajdasz ST, Christie RH, Carter C, Games D, Seubert P, et al. Imaging of amyloid-beta deposits in brains of living mice permits direct observation of clearance of plaques with immunotherapy. Nat Med 2001;7:369–72.

Bolmont T, Haiss F, Eicke D, Radde R, Mathis CA, Klunk WE, et al. Dynamics of the microglial/amyloid interaction indicate a role in plaque maintenance. J Neurosci 2008;28:4283–92.

Busche MA, Eichhoff G, Adelsberger H, Abramowski D, Wiederhold KH, Haass C, et al. Clusters of hyperactive neurons near amyloid plaques in a mouse model of Alzheimer's disease. Science 2008;321:1686–9.

Davalos D, Lee JK, Smith WB, Brinkman B, Ellisman MH, Zheng B, et al. Stable in vivo imaging of densely populated glia, axons and blood vessels in the mouse spinal cord using two-photon microscopy. J Neurosci Methods 2008;169:1–7.

Dombeck DA, Khabbaz AN, Collman F, Adelman TL, Tank DW. Imaging large-scale neural activity with cellular resolution in awake, mobile mice. Neuron 2007;56:43–57.

Dong J, Revilla-Sanchez R, Moss S, Haydon PG. Multiphoton in vivo imaging of amyloid in animal models of Alzheimer's disease. Neuropharmacology 2010;59:268–75.

Grutzendler J, Kasthuri N, Gan WB. Long-term dendritic spine stability in the adult cortex. Nature 2002;420:812–6.

Hadlock T, Kowaleski J, Mackinnon S, Heaton JT. A novel method of head fixation for the study of rodent facial function. Exp Neurol 2007;205:279–82.

Hefendehl JK, Wegenast-Braun BM, Liebig C, Eicke D, Milford D, Calhoun ME, et al. Long-term in vivo imaging of β-amyloid plaque appearance and growth in a mouse model of cerebral β-amyloidosis. J Neurosci 2011;31:624–9.

Holtmaat A, Bonhoeffer T, Chow DK, Chuckowree J, De Paola V, Hofer SB, et al. Long-term, high-resolution imaging in the mouse neocortex through a chronic cranial window. Nat Protoc 2009;4:1128–44.

Jin S, Bierschenk I, Naumann A, Lienkamp S, Groot E, Bensch R, et al. Advanced software for multi-purpose, intelligent confocal image recording, the ZEN macro library. In: Conference presentation, focus on microscopy; 2011.

Judkewitz B, Rizzi M, Kitamura K, Häusser M. Targeted single-cell electroporation of mammalian neurons in vivo. Nat Protoc 2009;4:862–9.

Kelly EA, Majewska AK. Chronic imaging of mouse visual cortex using a thinned-skull preparation|. JoVE 2010;44:e2060.

Meyer-Luehmann M, Spires-Jones TL, Prada C, Garcia-Alloza M, de Calignon A, Rozkalne A, et al. Rapid appearance and local toxicity of amyloid-β plaques in a mouse model of Alzheimer's disease. Nature 2008;451:720–4.

Nase G, Helm PJ, Reppen T, Ottersen OP. A multiphoton laser scanning microscope setup for transcranial in vivo brain imaging on mice. Rev Sci Instrum 2005;76:123702.

Nimmerjahn A. Resting microglial cells are highly dynamic surveillants of brain parenchyma in vivo. Science 2005;308:1314–8.

Sigler A, Murphy TH. In vivo 2-photon imaging of fine structure in the rodent brain: before, during, and after stroke. Stroke 2010;41:S117–23.

Spires-Jones TL, de Calignon A, Meyer-Luehmann M, Bacskai BJ, Hyman BT. Monitoring protein aggregation and toxicity in Alzheimer's disease mouse models using in vivo imaging. Methods 2011;53:201–7.

Trachtenberg JT, Chen BE, Knott GW, Feng G, Sanes JR, Welker E, et al. Long-term in vivo imaging of experience-dependent synaptic plasticity in adult cortex. Nature 2002;420:788–94.

Yang G, Pan F, Gan WB. Stably maintained dendritic spines are associated with lifelong memories. Nature 2009;462:920–4.

Yang G, Pan F, Parkhurst CN, Grutzendler J, Gan WB. Thinned-skull cranial window technique for long-term imaging of the cortex in live mice. Nat Protoc 2010;5:213–20.